
SPECT Dual-Energy-Window Compton Correction: Scatter Multiplier Required for Quantification

Kenneth F. Koral, Fayez M. Swailem, Steven Buchbinder, Neal H. Clinthorne, W. Leslie Rogers, and Benjamin M.W. Tsui

Division of Nuclear Medicine, Department of Internal Medicine, University of Michigan Medical Center, Ann Arbor, Michigan; and Department of Radiology, University of North Carolina, Chapel Hill, North Carolina

The dual-energy window Compton-scattering correction technique is defined here especially for accurate quantification of focal regions having higher than average uptake. The quantification is relative to a known-activity reference source. The scatter multiplier ("k" value) is determined for a radioactive ^{99m}Tc sphere on or off the axis of a cylinder containing water with or without background. Both maximum likelihood and filtered-backprojection reconstruction are employed. Either projections or tomograms are corrected. With tight regions of interest, there is a tendency for the requisite "k" value to be slightly lower as the diameter of the cylinder is increased. Neither sphere location nor background perturbs "k", however, so a constant value is a good, first approximation. Then a two-sphere validation test yields an accuracy of 8% with subtracted-tomograms ("k" = 1.30) and 2% with subtracted-projections ("k" = 1.20). With a reference-source region of interest which is four times larger, "k" is reduced and also now depends on background. Although equivalent quantitatively, maximum likelihood is preferable to filtered backprojection with Chang attenuation correction since it produces a less-noisy image.

J Nucl Med 1990; 31:90-98

One of the primary objectives of single photon emission computed tomography (SPECT) is to provide accurate quantitative cross-sectional images. The energy resolution of the sodium iodide used in Anger cameras is relatively poor (10-15% for the 140-keV photons emitted from the commonly used technetium-99m (^{99m}Tc) isotope), however, and an energy window of $\pm 10\%$ centered on the photopeak is normally used. The lower half of this window will receive photons which have undergone Compton scattering within the object through angles as large as 53° in addition to a significant number of doubly scattered photons (1). These scattered photons produce falsely positioned

events which should be removed by a scattering compensation technique for accurate quantification (2-5).

A comprehensive review of several techniques for Compton-scatter correction is given elsewhere (6). Developmental approaches include the analysis of the complete energy spectra at individual spatial locations in each view to separate the Compton-scattered component from the unscattered component (7), but this method has not been applied to patients. The dual-energy window method, originally proposed by Jaszczak et al. (8), is easy to implement in the clinic and has been shown to produce an improvement in image quality. In this method, data is acquired in two energy windows, a photopeak window and a low-energy scatter window, simultaneously, to collect two separate images. The assumption is made that the events detected in the scatter window are correlated to the scatter component of the events detected in the photopeak window in such a way that, for example, the image reconstructed from the scatter window can be multiplied by a factor "k" and subtracted from the image reconstructed from the primary window to effect scatter correction. In (8), attenuation correction using a linear attenuation coefficient $\mu = 0.15 \text{ cm}^{-1}$ was applied for both reconstructions. Also, a single value for the scatter multiplier, "k", equal to 0.5 was chosen by comparing a line source imaged in air to a SPECT reconstruction of the same source in water. The entire width of the image was included in the analysis rather than a restricted area. Since we are interested in accurate quantification of radiation absorbed dose delivered to focal patient tumors, as in the case of neuroblastoma patients undergoing metaliodobenzyl guanidine (MIBG) therapy or melanoma- and ovarian-cancer-cell patients who are undergoing diagnostic imaging with monoclonal antibodies, hot spot accuracy is our goal and a restricted region of interest (ROI) is used. Accordingly, the "k" in our case is expected to be different from that for cold spot imaging or unrestricted ROIs.

The general purpose of this research, then, is to study the behavior of the scatter multiplier required for ac-

Received Apr. 17, 1989; revision accepted Aug. 24, 1989.
For reprints contact: Kenneth F. Koral, PhD, University of Michigan Medical Center, 3480 Kresge III Bldg., Box 0552, Ann Arbor, MI 48109-0552.

curate quantification of simulated tumors which have uptakes higher than the average image region. There are two main aims: first, to investigate the effect of varying background levels around a spherical hot object on the “k” value and second, to relate the “k” value to “body-size” and “tumor-location” variation. In addition, the performance of different reconstruction algorithms with the same data is also tested. Finally, processing projection data by subtraction before reconstruction (SP mode) is compared to subtraction after reconstruction (ST mode). No tests of the effects of nonuniform attenuation are made.

MATERIALS AND METHODS

Theory

Because we are interested in correct quantification for hot finite-extent objects, we employ the following method (which is somewhat different from that in Reference 8) for obtaining the “k” value.

First, measure a “hot” sphere containing a known activity with the dual-window SPECT technique. Second, measure an attenuation-and-scatter-free source by the same method so all camera conditions remain the same, but retain only the direct-window data.

For absolute quantification in the subtracted-projection (SP) mode, make Assumption 1 (illustrated in Fig. 1):

The scatter counts within the direct window are correlated to the scatter counts within the scatter window by the same constant, “k”, for all pixels in all projections.

Then, if you know “k”, you can find the projection corrected for scattering, P, as follows:

$$P = P_D - k \cdot P_s, \quad (1)$$

where P_D is the projection obtained from the direct window and P_s is that from the scatter window. Since P now contains only full-energy events, it is obvious that reconstruction should use the full-energy attenuation coefficient for attenuation correction. The resultant number of total counts in the ROIs of the reconstructed images, C, and the camera efficiency, e, produce the final value for object activity, A:

$$A = \frac{C}{e}. \quad (2)$$

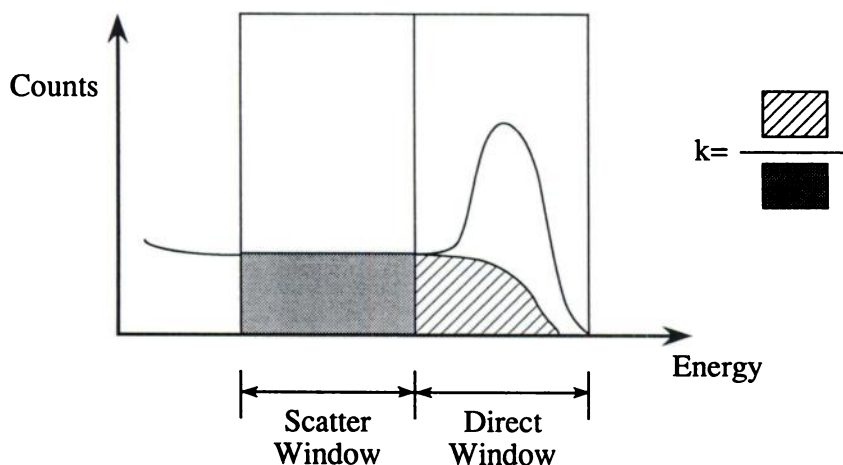


FIGURE 1
A sketch of the energy spectrum for a given pixel in a given projection. The counts in the direct window are composed of both scattered (lined area) and unscattered (white area) gamma rays. The counts in the scatter window are all lower-energy scattered gamma rays (cross-hatched area). By Assumption 1, the “k” value is the ratio shown.

The camera efficiency is assumed to be correctly and appropriately measured by reconstructing a scatter-free reference source without any correction for scatter or attenuation. The total counts within the ROIs, C_R , and the known activity, A_R , then give e:

$$e = \frac{C_R}{A_R}. \quad (3)$$

Since “k” itself is not originally known, the procedure shown in Figure 2 is used to obtain it with the SP mode. You first choose a “k” value you hope to be near the correct value. From this value and Equations (1) through (3), you can find a value for the sphere activity, A, associated with that “k” value which we will call A_k . Since the true activity, A_t , is known, the error in the calculated activity, Δ_k , can be found:

$$\Delta_k = A_t - A_k. \quad (4)$$

One then chooses a second, significantly-different “k” value and repeats the procedure. By plotting Δ_k versus k, as shown in Figure 2, one interpolates to find the “k” value which produces correct quantification (it corresponds to a Δ_k value of zero).

With the subtracted tomogram (ST) mode, that was also used in Reference 8, one again starts with Equation (3). One then makes a different assumption, which we will call Assumption 2, namely:

$$A = \frac{C_D - k \cdot C_s}{e}, \quad (5)$$

where C_D is the sum of the counts within the ROIs for the object found in the tomograms from the direct-window data and C_s is that within the same ROIs in those from the scatter-window data.

From Equations (3) and (5) we obtain the “k” value required for accurate quantification of a known activity A as:

$$k = \frac{d - e}{s} \quad (6)$$

after having made the definitions below:

$$d = \frac{C_D}{A} \quad (7)$$

$$s = \frac{C_s}{A}$$

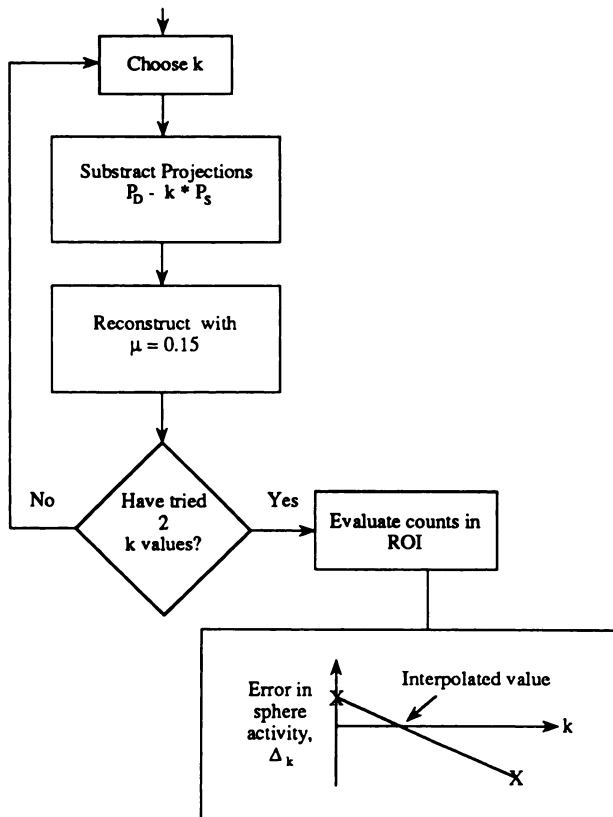


FIGURE 2
Flow chart for the Subtracted Projections, SP, mode to obtain the “k” value with zero error in the calculated activity. P_D and P_S are the projections obtained with the direct and the scatter window, respectively.

Here, the tomograms are reconstructed with attenuation coefficients that could correspond to different energies for the scattered and direct windows. However, we follow Reference 8 and use the same, full-energy value for both reconstructions.

Since there is an arbitrariness in the attenuation correction with the ST mode, our choice may not result in the same “k” values as with the SP mode. Although the two modes may require different “k” values, they both may produce acceptable quantification for a wide range of objects when the value appropriate to the mode is used.

After one has obtained the “k” and “e” values by either the ST or SP method, then unknown tumor activities can be evaluated. In SP mode, Equations (1) to (3) are employed with “A” now referring to tumor activity and “C” being counts within the tumor ROIs. In ST mode, Equations (3) and (5) are used. In either mode, the camera efficiency can be reevaluated at the time of imaging, or the value obtained at the time the “k” value was obtained can be reused.

Phantom Testing

In all, two cylindrical phantoms (Data Spectrum Corporation, Chapel Hill, North Carolina) were used. The diameter of the first was larger (22.2 cm outside diameter and 18.6 cm inside height) and that of the second smaller (20.5 cm outside diameter and 25.4 cm inside height). A sphere (6.0 cm diameter) was placed inside the cylinder supported by a plastic rod.

In the first experiment, ^{99m}Tc solution was used for the

sphere and for the cylinder (as a background). Sphere activity was kept constant (except for decay) while that of the cylinder was increased. The ratio of the specific activity, in $\mu\text{Ci/ml}$, of the cylinder over that of the sphere was thus varied from 0, i.e., hot sphere in a cold cylinder to 1, i.e., specific activity of the sphere equal to that of the cylinder. The last case was accomplished by reconstructing the acquired data of the highest background study below the sphere level, i.e., for the cylinder activity only. The specific activity of the sphere was $\sim 4.4 \mu\text{Ci/ml}$ while that of the cylinder varied from 0 to $0.54 \mu\text{Ci/ml}$.

In the second experiment, the position of the sphere was varied between “on axis” and “off axis” in both cylinders. The “off-axis” position for each cylinder places the sphere center 5.7 cm from the axis of the cylinder. The same sphere and activity were utilized as in experiment 1, but decay had reduced the sphere specific activity to $\sim 0.5 \mu\text{Ci/ml}$.

In addition to phantom imaging, a reference source was also used. This source was prepared by homogeneously distributing 0.11 mCi of ^{99m}Tc over a 2.0 cm diameter filter paper. It was taped to the camera collimator at the center. Acquisition was as for the phantom and reconstructions were also the same except that no attenuation correction was applied due to absence of a scattering medium. Since it was in a fixed position in the projection images, the reference source reconstructed approximately as a spherical shell and thus was similar in shape to the spheres for which it was the calibrator of camera efficiency. The syringes for all sources had their activities assayed in a dose calibrator.

Two Sphere Validation

To test the accuracy of our conclusions about what scatter multiplier to employ for quantification of tumors, a final phantom experiment was conducted. A 6-cm-diameter sphere with a known amount of activity was placed off-axis in the large-diameter cylinder. Then, a second sphere of the same diameter and containing approximately the same activity was added to the cylinder to simulate a nearby organ. This sphere was also off-axis and was 120° from the first sphere. The phantom containing the two spheres was imaged in the same way as in the other studies.

Camera and Data Acquisition

A GE “Maxi Camera II” (General Electric, Milwaukee, Wisconsin) with a half-inch-thick crystal and a general purpose low-energy collimator were employed. The camera was interfaced to a GE STAR computer. A dual-energy window tomographic acquisition for the phantoms and the reference source was accomplished. The direct window was set at 124–154 keV (nominally 20%) and the scatter window was set just below it at the same width (93–123 keV). Acquisitions were taken over 64 angles with 20 sec per view and spatial resolution of 64×64 word. A previously-acquired energy map of the variation of energy pulse height across the face of the crystal obtained with a ^{99m}Tc source was used to correct the energy signals. This pulse-height correction is a part of the autotune feature of the camera.

Also, a 30 million count flood, obtained from a ^{99m}Tc source, for the direct window was evaluated to provide uniformity correction for the projection images for each window. This correction was made to the computer-stored data either on-line or after acquisition.

Deadtime Correction

To obtain quantitative information at different counting rates, we corrected our data for the temporal resolution of the camera, i.e., for counting rate losses due to deadtime (9,10). The deadtime correction factor was measured for both energy windows for each individual study using a monitor source. This source was taped to the collimator face out of the interesting part of the field-of-view and then covered with lead to intercept gamma rays from the main object. The monitor source contained $\sim 250 \mu\text{Ci}$ of $^{99\text{m}}\text{Tc}$ homogeneously distributed over a 3.5-cm-diameter filter paper. It was covered by 1.59-mm-thick lead sheet. The monitor source was measured by itself without the phantom at a given recorded time and then measured again with the phantom in place. After decay correction, the measured deadtime correction factor is the ratio of the monitor-source count rate alone over that with the object.

Reconstruction Algorithms

The scatter multiplier required for accurate tumor quantification was evaluated for three reconstruction algorithms. These are: (a) iterative maximum likelihood (ML) with a map of attenuation coefficients (11); (b) filtered backprojection (FBP) after analytic correction of projections for attenuation; and (c) filtered backprojection, followed by Chang attenuation correction (12) using a map of attenuation coefficients (FBPC) (13). This FBPC procedure was capable of being employed in an iterative manner.

Iterative Reconstruction

Raw data were transported to a VAX 7500/VAX 8300 cluster for ML and FBPC reconstruction. Neither algorithm requires an assumption of a uniform attenuation coefficient, although that assumption with an attenuation coefficient of 0.15 cm^{-1} was made for these phantoms. The FBPC program used the same attenuation maps as ML. A slice width equal to 3 pixels in the z direction was selected in ML and FBPC reconstructions for both phantom and reference source studies in order to reduce the number of slices in which ROI had to be found.

Attenuation Maps

The correct sizing and location of a uniform attenuation map was expected to be important for these studies. When there was background activity in the cylinder, we first reconstructed the direct-window data with no attenuation correction. The map was determined by the edges of the circular image, defined approximately by a drop in the count level to 50% of the maximum near the edge. Without background, the same approach was used on the reconstruction of the scatter-window data. Here, however, the edge was less defined and so the assessment of the map center was made with less confidence in its accuracy. To test the importance of the map placement, one reconstruction was repeated with a total of 5 maps and the k value computed for each.

FBP Reconstruction

For standard FBP reconstructions, raw data were transferred to an MDS A² computer. A high-resolution "ramp-Hanning" filter was utilized. The projections were precorrected for attenuation with a multiplicative factor calculated for each projection element by knowing the true object distribution.

Regions of Interest

All tomograms were either present or transferred to the A² computer for analysis and evaluation. Reference source ROIs were determined from a semi-automatic, second-derivative-based program. The same program was applied to the no-background, big-cylinder sphere to produce a size for the sphere ROIs in each of four planes. Due to variations in behavior of the program, the same size ROIs did not occur for other sphere images. To keep the sizes consistent, hand drawing was resorted to when studying parameters such as the level of cylinder background so as to isolate the effect of the parameter. During these same parameter variations, a single reference source determination was used. Measurements were sufficiently close together in time to assume that there was no camera variation during the course of the experiment which would have required a new reference-source calibration.

To determine the effects on the "k" value of choosing larger ROIs than the "automated" ones described above, we (a) expanded the sphere ROI to one with four times the area of the "automated" ROI and (b) we separately did the same for the reference-source ROI. The effect of the change on the requisite "k" values was calculated.

One could also consider using larger-size sphere ROIs in the scatter image than in the direct image. This choice would be reasonable because resolution is known to be worse in the scatter image. However, it would involve twice the number of ROIs. More importantly, in clinical images there is often activity near the tumor, so using the minimum-size, meaningful ROIs is necessary to avoid the influence of this variable activity.

Horizontal and vertical profiles through the reconstructed images were used to visually assess noise.

RESULTS

Number of Iterations

Both ML and FBPC are iterative algorithms and their output is, in general, dependent on the number of iterations. For the ML algorithm, 16 iterations were required before quantitative results were not changing further within 1% to 2%. For the FBPC algorithm, convergence was very rapid. This fact was shown by examining the hot sphere results with increasing cylinder background activity. For the direct-window tomograms, 16 iterations added $\sim 2\%$ more counts within the sphere's ROI than 1 iteration when the ratio of specific activity in the cylinder over that in the sphere was 0.00. This percent decreased to 1% for the case of the specific activity ratio equal to 0.09. For the scatter-window, the difference was insignificant. However, examination of profiles taken over the reconstructed images found more noise in the uniform-activity region for the case of 16 iterations compared to one iteration. For this reason, we restricted our FBPC reconstructions to one iteration.

Deadtime Correction

Using the monitor source method, it was found that for the direct window, the deadtime-correction factor increased linearly with increasing average total counts

TABLE 1
Effect of Attenuation Map Shift on the Scatter Multiplier

Map placement	Specific counts scatter-window k counts/mCi	Specific counts direct-window k counts/mCi	"k" Value
Original map	35	149	1.22
Shift 1 pixel right, 1 pixel up	37	158	1.40
Shift 1 pixel right, 2 pixels up	39	167	1.57
Shift 1 pixel right, 3 pixels up	41	176	1.74
Shift 1 pixel right, 4 pixels up	43	184	1.89

per projection in the range between 0 to 10 kcts/sec. The correction factor varied between 1.00 and 1.10. This result agrees with the paralyzable (nonextendable) deadtime model that fits most scintillation cameras. For the scatter window, however, the correction factor behaved in an erratic manner. Independent measurements on deadtime later confirmed that the monitor source is inaccurate for the scatter window while data for both windows fit the same model with almost the same parameters. Therefore, the count rate averaged over angle was calculated for the scatter window and used as the independent variable in the linear relationship for the direct-window correction factor. In this way, a correction factor varying between 1.00 and 1.06 was obtained for the scatter-window data. In ST mode, the values of "C_D" and "C_S", in Equation (5), are corrected by the corresponding factors.

In SP mode, these corrections are applied to the separate projection data sets before reconstruction.

Effect of Attenuation-Map Placement

To demonstrate the effect of attenuation map placement on the "k" value, five map positions for the "large-diameter cylinder, off-axis, 0.00-specific-activity-ratio" study were tested. The results from the ML reconstruction are given in Table 1.

As the map was shifted over or up so the off-axis sphere (located at approximately 12 o'clock) tended to be nearer the center of the attenuating medium, both scatter and direct counts increased, but the latter more rapidly. Therefore, the k value increased at the rate of ~0.17 per pixel of map displacement. This large rate highlights the importance of correct map placement.

Variation of "k" Value with Specific Activity Ratio

The results for the hot sphere located "off-axis" in the "large-diameter" cylinder filled with water containing increasing amounts of radioactivity are shown in Figures 3 and 4. The sphere specific counts (kcts/1 mCi) for the scatter and direct window tomograms using ML are plotted against the specific activity ratio in Figure 3. Both relations are straight lines which confirms that the attenuation maps have been correctly located.

The results for the "k" value using different specific

activity ratios are given in the first six rows of Table 2. Figure 4 is a plot of the "k" value versus the specific activity ratio using ML and SP mode. The solid line is at the level of the average value of 1.22. Although there may be some more complicated form to the dependency, to first order, our results are consistent with "k" being independent of background.

Effect of Cylinder Size and Sphere Location

When there is no cylinder activity, the effect of cylinder size and sphere location on the "k" value is given by rows 1, 7, 8, and 9 of Table 2. The results using ML in SP mode are illustrated in Figure 5 with a solid line representing the average value. The standard deviation from this average value is only 2.7% so the choice of a single "k" value for these cases would not lead to large errors.

On the other hand, inspection of all pertinent data in Table 2 reveals a trend for the requisite scatter multiplier to be slightly lower for the large cylinder than for the small cylinder. Averaging results over the ML and FBPC algorithms, "k" is 10% lower in ST mode and 4.0% lower in SP mode. Likewise, it is 5.6% lower

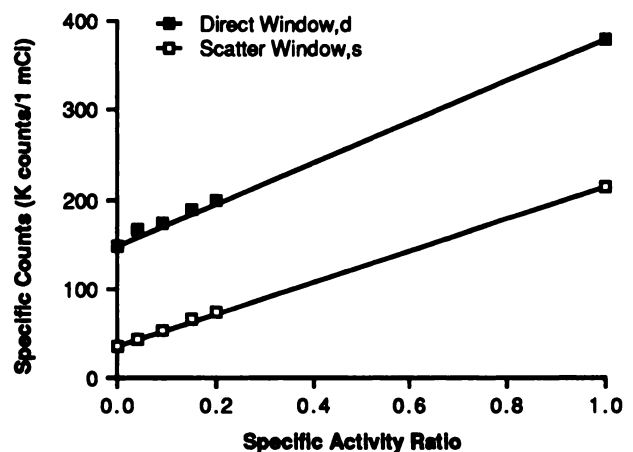


FIGURE 3
A plot of specific counts versus specific activity ratio (specific activity of cylinder/specific activity of the sphere) for the direct and the scatter window tomograms using ML algorithm and ST mode. The straight line relationship for both windows verifies the accurate location of the attenuation maps for these studies.

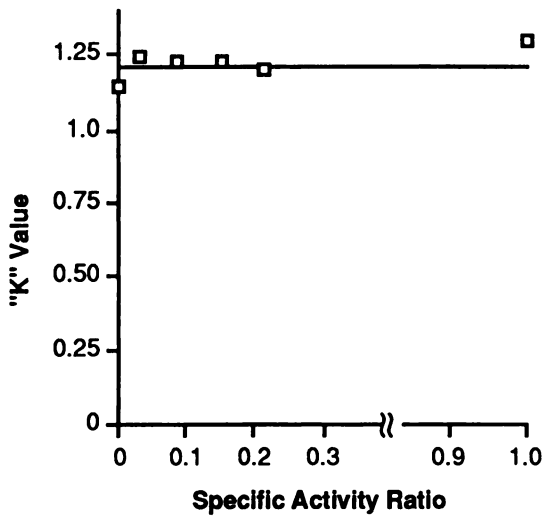


FIGURE 4
Relationship between the “k” value and the specific activity ratio (cylinder over sphere) using ML algorithm and SP mode for a sphere with constant activity located off-axis in the large-diameter cylinder filled with increasing background activity. To first order, our results are consistent with “k” being independent of the level of cylinder background.

in the case of FBP (ST mode). Thus, there is an indication that an investigation with a larger range of sizes for the cylinder would show that the scatter multiplier needed for quantification decreases as the cylinder diameter increases.

The observed trend can be explained as follows. Let the direct-window scatter fraction be the number of scattered events within the direct window divided by the number of unscattered gammas in that window and

the scatter-window scatter fraction be the number of scattered gammas within the scatter window divided by the same denominator. Most probably, both scatter fractions increase as the cylinder diameter increases. However, our result (“k” smaller for the larger cylinder) is explained by the direct-window scatter fraction going up more slowly than the scatter-window scatter fraction. Thus a smaller multiplier is needed to compensate.

One also sees, from Table 2, that once a mode is chosen, then there is agreement between the ML and FBPC algorithms. On the other hand, there is a tendency for the ST mode to require a higher “k” value for accurate quantification. With no background, the average value for all geometries and for both algorithms using ST mode is 1.31 ± 0.09 while for SP mode it is 1.15 ± 0.03 . The reason for the dependence of the results on mode is most likely the difference between Assumptions 1 and 2 (see Theory section). Note that with subtracted projections, only accurate quantification in the final result has been required; the detailed accuracy of Assumption 1 has not been tested or verified.

Two-Sphere Validation

Results of the validation study for the two iterative algorithms are shown in Table 3. The “k” value employed is the average over all studies and both iterative algorithms for a given mode. It is seen that without Compton-scatter correction, the error in calculated activity is large (~60%) while with correction it is much reduced. In fact, in the subtracted-projections mode, it is 2% or less independent of algorithm type.

TABLE 2
The “k” Value Versus Sphere Location, Cylinder Size, and Activity for Three Algorithms and Two Modes: “Automated” ROIs

	Cylinder diameter	Specific location	Specific-activity ratio	ML		FBPC		FBP ST
				ST	SP	ST	SP	
1*	Large	Off-axis	0.00	1.21	1.11	1.20	1.11	1.18
2	Large	Off-axis	0.04	1.33	1.24	1.35	1.24	1.29
3	Large	Off-axis	0.09	1.27	1.23	1.31	1.23	1.28
4	Large	Off-axis	0.15	1.25	1.23	1.28	1.23	1.28
5	Large	Off-axis	0.20	1.22	1.20	1.25	1.22	1.25
6	Large	Off-axis	1.00	1.31	1.30	1.32	1.32	1.41
7	Large	On-axis	0.00	1.29	1.15	1.27	1.15	1.17
8	Small	Off-axis	0.00	1.38	1.17	1.37	1.19	1.24
9	Small	On-axis	0.00	1.40	1.18	1.38	1.17	1.25
	Average value			1.30 ±0.06	1.20 ±0.05	1.30 ±0.06	1.21 ±0.06	1.26 ±0.07

ML = maximum likelihood reconstruction algorithm.
 FBPC = filtered backprojection plus Chang attenuation correction.
 FBP = filtered backprojection reconstruction algorithm.
 ST = subtracted tomograms mode.
 SP = subtracted projections mode.
 * Average values from three runs at different times.

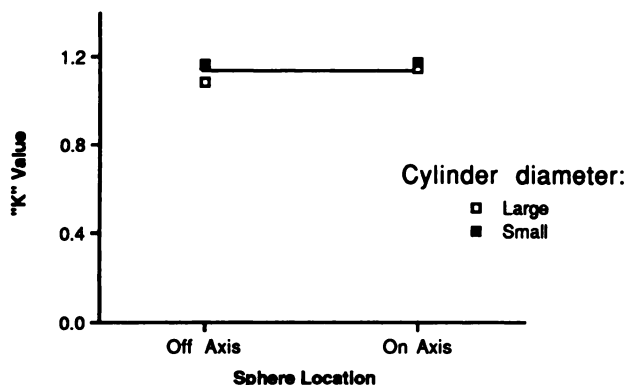


FIGURE 5
This figure illustrates the effect of cylinder size and sphere location on the "k" value using the ML algorithm and SP mode. The solid line represents the average value. Choosing this average for the scatter multiplier would be a good first approximation. The smaller cylinder, however, does show slightly higher "k" values.

Effect of Size of ROIs

Very large ROIs (4 times that of the "automated" method) have the following effects. The variation in the absolute value of "k" is shown in Table 4 for the large cylinder on axis with no background and ML reconstruction (ST mode). It is seen that with the large reference-source ROI in combination with the "automated" sphere ROI, k decreases to a value of 0.73.

The fact that not only the absolute value of "k" but also its dependence on activity-distribution is affected by the size of the reference-source ROI is shown in Table 5. For ML reconstruction in ST mode, the requisite "k" now increases monotonically as the background-to-sphere specific-activity ratio increases. For any of the tested combinations of mode and algorithm, the behavior is of the same form. Using FBP and the ST mode (not listed), the requisite "k" value increases from an all-study low of 0.38 to 1.25.

Qualitative Effects

The choice of the reconstruction algorithm has little effect on the average "k" value for the different studies when the ROIs are the small, "automated" ones. Yet,

TABLE 3
"Tumor" Accuracy

Algorithm or parameter	Activity error*		
	No Compton correction	Compton-correction mode	
		ST	SP
"k"	0.00	1.30	1.20
FBPC	+61%	+7.8%	+2.0%
ML	+62%	+7.9%	+1.1%

* Error = $\frac{\text{Calculated} - \text{True}}{\text{True}} \cdot 100.$

TABLE 4

Value of "k" for Different Combinations of ROI Choice. Sphere on Axis, Large Cylinder, No Background, ML Algorithm, and ST Mode

Sphere ROI	"automated" large	Reference-source ROI	
		"automated" (e = 0.11)*	large (e = 0.13)*
Sphere ROI	"automated" large	1.29	0.73
	large	1.30	0.98

* The camera efficiency value for a 64 stop, 20 sec per stop, acquisition in units of million counts per millicurie.

even then it has a recognizable effect on the quality of the reconstructed images. Figure 6 shows a reconstructed slice through the middle of the sphere for the 0.20 specific activity ratio study comparing ML and FBPC. A vertical profile for both images located at the same coordinate shows a smoother pattern in the ML reconstruction and a noisier pattern in FBPC reconstruction. This result agrees with Reference 13.

DISCUSSION

Our results indicate that for ^{99m}Tc and using "tight" ROIs, a single "k" value can be chosen and reasonably accurate results obtained for a variety of geometrical and background conditions. The value depends on the reconstruction method and is that listed on the last line of Table 2. There is some indication that, for greater accuracy, some dependency of "k" on body size (and perhaps on shape, although shape wasn't investigated here) should be established.

Filtered backprojection produces acceptable results when the projections are corrected before reconstruction by a method which depends on knowing the activity distribution. Such an approach could lead to a clinically useful, iterative algorithm but that remains to be shown. Filtered backprojection followed by Chang attenuation correction leads to satisfactory quantitative accuracy (even in only one iteration). Here, however, the reconstructed image is noisy outside the sphere. Therefore, ML reconstruction seems to be the method

TABLE 5

The "k" Value Versus Cylinder Activity for "Automated-Sphere and Large-Reference-Source ROIs. Off-Axis Sphere, ML Reconstruction and ST Mode

	Specific-activity ratio	"k" Value for correct quantification
1	0.00	0.62
2	0.04	0.84
3	0.09	0.86
4	0.15	0.91
5	0.20	0.93
6	1.00	1.21

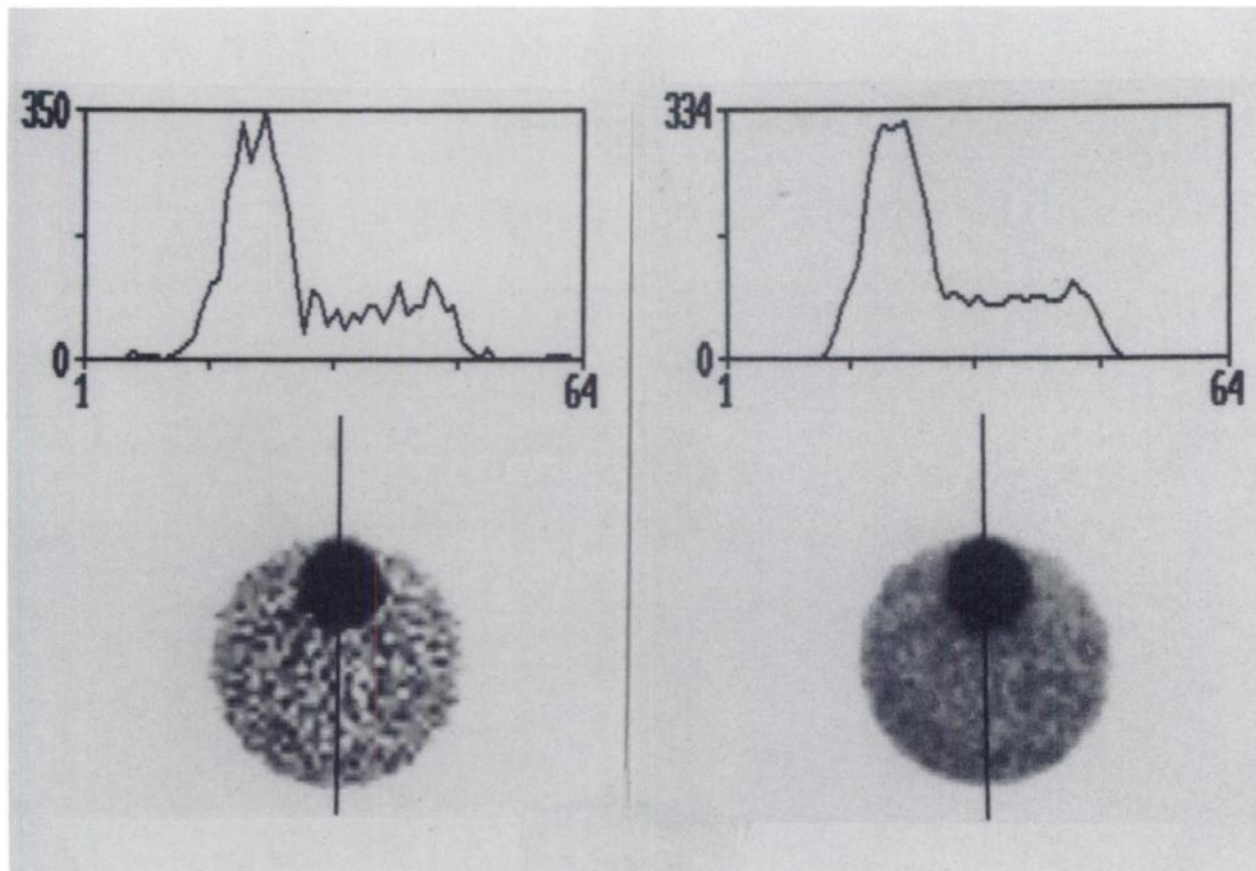


FIGURE 6
Reconstructed slices through the middle of the sphere for the study with a 0.20 specific activity ratio. At left is a vertical profile through the middle of the sphere using FBPC, and at right is the same profile for ML. ML shows a less noisy result.

of choice. In one verification test, this algorithm gives good results. Its use in subtracted-projections mode is superior to that in subtracted-tomograms mode for that test, but it isn't known whether that superiority would hold over a larger range of situations.

The application of the basic method to quantification in cold-spot imaging is possible. The ordinate or specific-activity ratio in Figure 4 would then be extended beyond 1.0 towards infinity. It isn't possible to predict the behavior of the "k" value there from present results.

With our data, we have also shown that the "k" value is reduced from 1.29 to 0.73 by choosing a much larger ROI for the reference source. It is likely that the "k" value of 0.5 previously reported by Jaszczak et al. would increase (and thus be closer to our values) if their ROIs were made smaller. Also, in cardiac imaging with ^{99m}Tc , Galt has found his best agreement for experimental versus expected counts over a range from 6,000 to 12,000 with a "k" of 1.0 (14) rather than 1.2–1.3 or 0.5. Therefore, values from different investigations do not disagree so much as depend exactly on the defined method.

Finally, we could have assumed a model in which part of the direct-count spectrum tailed into the scatter window. Such a choice changes the formulation and

the resultant "k" values. It potentially could unfavorably affect the constancy of "k" when using the "automated" ROIs. We feel the present model is a good choice.

Extension of the method to other isotopes could be carried out. One could, in fact, assume that with the "automated" ROIs the approximate independence of "k" from background and geometry is the same as found here for ^{99m}Tc . Then, a single measurement of a hot sphere in a cold cylinder would determine the appropriate "k" value for the new gamma ray with its new windows and changed scattering cross sections due to different energy.

Further measurements on the effect of several parameters on the scatter multiplier required for quantitative imaging are also possible. These parameters include: (a) body size, an extension of present measurements, (b) body shape, (c) size and shape of tumor, (d) nonuniform attenuation, and (e) nonuniform background distribution.

ACKNOWLEDGMENTS

This work was supported by PHS Grant Numbers CA38790 and 5 T32 CA09015 awarded by the National Cancer Institute,

DHHS. The authors thank Jill Anderson for secretarial assistance in preparation of the manuscript and Eric R. Edgerton, David R. Gilland, and Hon-Bin Hu for assistance with the computer programs.

REFERENCES

1. Floyd CE, Jaszczak RJ, Harris CC, Coleman RJ. Energy and spatial distribution of multiple order Compton scattering in SPECT: a Monte Carlo investigation. *Phys Med Biol* 1984; 29:1217-1230.
2. Beck RN, Schuh MW, Cohen TD, et al. Effects of scattered radiation on scintillation detector response. *Med Radioisotope Scintigraphy IAEA (Vienna)* 1969;595-616.
3. Axelsson B, Maski P, Israelsson A. Subtraction of Compton-scattered photons in single photon computed tomography. *J Nucl Med* 1984;25:490-494.
4. Oppenheim BE. Scatter correction for SPECT. *J Nucl Med* 1984;25:928-929.
5. Lowry CA, Cooper MJ. The problem of Compton scattering in emission tomography: a measurement of its spatial distribution. *Phys Med Biol* 1987;32:1187-1191.
6. Jaszczak RJ, Floyd CE, Coleman RE. Scatter compensation techniques for SPECT. *IEEE Trans Nucl Sci* 1985; NS-32:786-793.
7. Koral KF, Wang X, Rogers WL, Clinthorne NH, Wang X. SPECT Compton-scattering correction by analysis of energy spectra. *J Nucl Med* 1988;9:195-202.
8. Jaszczak RJ, Greer KL, Floyd CE, Harris CC, Coleman RE. Improved SPECT quantification using compensation of scattered photons. *J Nucl Med* 1984;25:893-900.
9. Adams R, Hine GJ, Zimmerman D. Deadtime measurement in scintillation cameras under scatter conditions simulating quantitative cardiology. *J Nucl Med* 1978;19:538-544.
10. Gulberg C, Rossing N. Comparing the performance of two gamma cameras under high counting rates: principles and practice. *J Nucl Med* 1978;19:545-552.
11. Shepp LA, Vardi Y. Maximum likelihood reconstruction for emission tomography. *IEEE Trans Med Imag* 1982;MI-1:113-132.
12. Chang LT. A method for attenuation correction in radionuclide computed tomography. *IEEE Trans Nucl Sci* 1978; NS-25:638-643.
13. Tsui BMW, Hu HB, Gilland DR, Gullberg GT. Implementation of simultaneous attenuation and detector response correction in SPECT. *IEEE Trans Nucl Sci* 1988; NS-35:778-783.
14. Galt JR. Reconstruction of the absolute radionuclide distribution in a scattering medium from scintillation camera projections. PhD Dissertation, Emory University, Department of Physics, 1988. University Microfilm. Ann Arbor, MI, 237 pp.